A robust algorithm for calculating the spatial deformations of rods without tensile strength

András A. Sipos

Department of Mechanics, Materials and Structures, and Center of Applied Mathematics and Computational Physics, Budapest University of Technology and Economics, 1111 Budapest, Műegyetem rkp. 3, Hungary; sa128@hszk.bme.hu

Abstract. A globally convergent iterative algorithm for computing the spatial deformations of elastic beams without tensile strength is presented. The core of the algorithm is an iterative scheme (consistent with the classical Kirchhoff rod theory) for locating the neutral axis and thus for determining the curvature. We prove uniqueness and local stability for the general case and global stability for symmetric cross sections. The scheme is embedded in an iteration-free global boundary value problem solver (the so-called Parallel Hybrid Algorithm) to determine spatial equilibrium configurations. The obvious applications are steel reinforced concrete beams and columns, with or without pre-stressing.

Key words: spatial deformations, steel reinforced concrete rod, asymmetric loading, Parallel Hybrid Algorithm, global convergence.

1. INTRODUCTION

The literature on spatial deformations of elastic rods is rich and growing. These works are not only inspired by the engineering praxis [1–5], but concern also the mechanical modelling of the DNA [6,7] and other biological phenomena [8,9]. Apparently no mathematically consistent, convergent algorithm is available for beams without tensile strength. Such beams, subjected to bending moments, *crack* on the tensile side, i.e., the shape of the actual cross section is determined by the acting forces and moments. The best known and most obvious examples are reinforced concrete beams which develop cracked zones already under service loads, i.e., in the elastic range.

One key problem is finding the actual shape of the cross section, assuming that the acting forces and moments are determined. The literature on reinforced

concrete offers methods for achieving this goal [10]. These methods rely on general nonlinear solvers (e.g. the Newton–Raphson method), thus no information is available on the global convergence features. In fact, one can find examples of divergent iterations [10]. In Section 2 we describe a direct recursion, which appears to be not only rather natural (is derived directly from the equilibrium equations and consistent with the classical Kirchhoff rod theory) but also globally convergent. We prove global uniqueness of the equilibrium solution and its local (super)stability. Global convergence can be proven for symmetric cross sections, however, we are convinced that a similar mechanism is governing the asymmetric, general case. For the latter, we ran systematic numerical trials and found the method in all (even extreme) cases to display robust and very fast convergence.

Once the shape of the cross section (also that of the cracked zone) has been identified by the above mentioned iterative scheme, the curvatures are readily obtained and the shape of the beam as an *initial value problem* (IVP) can be found via simple forward integration. Already for the IVP solution it is essential that the cracked zone should be computed in a rapid and convergent manner, otherwise the integration is unduly delayed or even halted (in case of divergence). To identify equilibrium shapes, one has to solve a *boundary value problem* (BVP). We use the Parallel Hybrid Algorithm (PHA) [11,12] described in Section 3 for this purpose. The PHA is not a continuation code, i.e., it is capable of identifying disconnected equilibria as well. Such configurations can be relevant when the structure snaps from one configuration to another. One has to pay high computational toll for the detection of disconnected equilibria; this is partially compensated by the parallel features of the PHA. We embedded the iterative scheme into the PHA. Since the scheme showed fast, global convergence and the PHA does not include iterative steps, the combined method proved to be very robust. Section 4 summarizes our results.

2. A CONVERGENT SCHEME FOR LOCATING THE NEUTRAL AXIS

2.1. Description of the scheme

We consider a cross section of arbitrary shape, assuming that the acting forces and bending moments are determined. The section consists of two elastic components: the regions without tensile strength called "*concrete*" and the regions with a symmetrical material law called "*reinforcement*". Locating the neutral axis is a highly nonlinear problem, since the unknown neutral axis is the boundary of the working (i.e. compressed) concrete area. In the literature general nonlinear solvers (such as Newton–Raphson and Quasi Newton methods), or FEM methods are used to determine the neutral axis. We propose a direct recursion based on equilibrium conditions. Our method can be associated with a two-dimensional map.

A compressive force F is applied at the point P (Fig. 1). Since the proposed method determines a physically objective quantity, namely the neutral axis, the iterative process does not depend on the applied coordinate system. To avoid coordinate transformations and to have a relatively simple form, we use a *global* $[XY]$ coordinate system, which is a freely chosen coordinate system having the origin at the point P. The quantities measured in a global coordinate system are always denoted by capital letters.

Let $f(\varepsilon)$ denote the stress–strain relation for the concrete and $g(\varepsilon)$ be the stress–strain relation of the reinforcement. We assume

$$g(\varepsilon) = nf(\varepsilon), \tag{1}$$

where n is a positive constant.

A_c and A_rf denote the areas of the actual concrete and the reinforcement, respectively. At each step of the iteration we calculate the neutral axis assuming (temporarily) that the concrete has tensile strength. The stress–strain relation for this case is denoted by $f'(\varepsilon)$, where $f'(\varepsilon) = f(\varepsilon)$ if $\varepsilon > 0$ and $f'(\varepsilon) = -f(-\varepsilon)$ if $\varepsilon < 0$ (Fig. 2). After identifying the ith estimate on the neutral axis inter-secting X and Y at X^i and Y^i, respectively, the total area of reinforcement A_rf and the compressed concrete area A_c define the "active" part of the cross section, which is the input of the $(i+1)$st step of the recursion. Accepting the hypothesis of plane cross sections, we can express the strains as

$$\varepsilon = x\cos(\alpha) + y\sin(\alpha) - t, \tag{2}$$

$$\alpha = \arctan(Y^i / X^i), \qquad t = \frac{X^i Y^i}{\sqrt{X^{i^2} + Y^{i^2}}}. \tag{3}$$
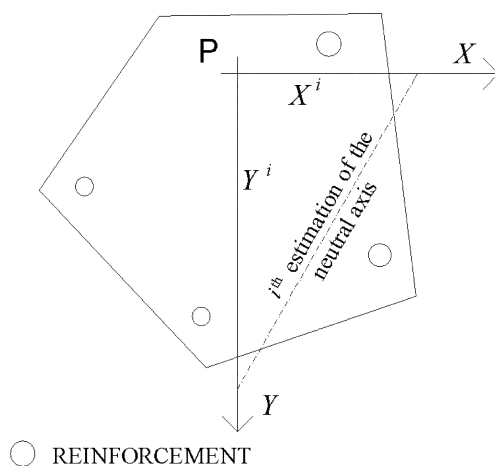
Fig. 1. The applied signs.
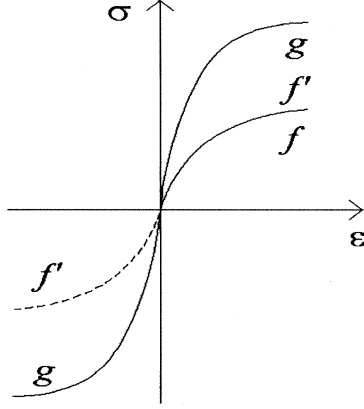
Fig. 2. The stress–strain relations.

The equations of equilibrium are the following:

$$\int_{A_c} f'(\varepsilon)\mathrm{d}A + \int_{A_{rf}} g(\varepsilon)\mathrm{d}A = F, \tag{4}$$

$$\int_{A_c} xf'(\varepsilon)\mathrm{d}A + \int_{A_{rf}} xg(\varepsilon)\mathrm{d}A = 0, \tag{5}$$

$$\int_{A_c} yf'(\varepsilon)\mathrm{d}A + \int_{A_{rf}} yg(\varepsilon)\mathrm{d}A = 0. \tag{6}$$

As long as

$$f(\varepsilon) = c \cdot \varepsilon^k, \tag{7}$$

where c and k are positive constants, the location of the neutral axis does not depend on the absolute value of the load F, i.e., Eq. (4) is independent of (5), (6). In this case the general form of the recursion can be given as

$$\begin{bmatrix} X^i \\ Y^i \end{bmatrix} = \begin{bmatrix} F(X^{i-1}, Y^{i-1}) \\ G(X^{i-1}, Y^{i-1}) \end{bmatrix}, \tag{8}$$

where $F(X,Y)$ and $G(X,Y)$ are derived from Eqs (5) and (6). If k is an integer, the functions F and G can be given in a closed form. In case of linear elasticity ($f(\varepsilon) = c\varepsilon$), F and G can be expressed explicitly as

$$\begin{bmatrix} X^i \\ Y^i \end{bmatrix} = \begin{bmatrix} F(X^{i-1}, Y^{i-1}) \\ G(X^{i-1}, Y^{i-1}) \end{bmatrix} = \begin{bmatrix} \dfrac{(D_{xy}^{i-1})^2 - I_x^{i-1} I_y^{i-1}}{D_{xy}^{i-1} S_x^{i-1} - I_x^{i-1} S_y^{i-1}} \\[2ex] \dfrac{(D_{xy}^{i-1})^2 - I_y^{i-1} I_x^{i-1}}{D_{xy}^{i-1} S_y^{i-1} - I_y^{i-1} S_x^{i-1}} \end{bmatrix}, \qquad (9)$$

where S_x, S_y, I_x, I_y, D_{xy} are the first and second moments of the area of the actual cross section, respectively.

The method starts with a first estimate on the neutral axis. The area of the reinforcement with the part of the concrete cross section bordered by the first estimation and containing the load is called the working cross section part. Equation (9) is solved by defining a new neutral axis. This line and the original cross section are the input of the next step of the iteration. We continue this recursion until the distances of two neutral axes in the following steps are smaller than an arbitrary small δ.

In numerical simulations we found that the two-dimensional map given in Eq. (9) is globally convergent. Since a two-dimensional map is typically chaotic, the global convergence requires detailed investigation.

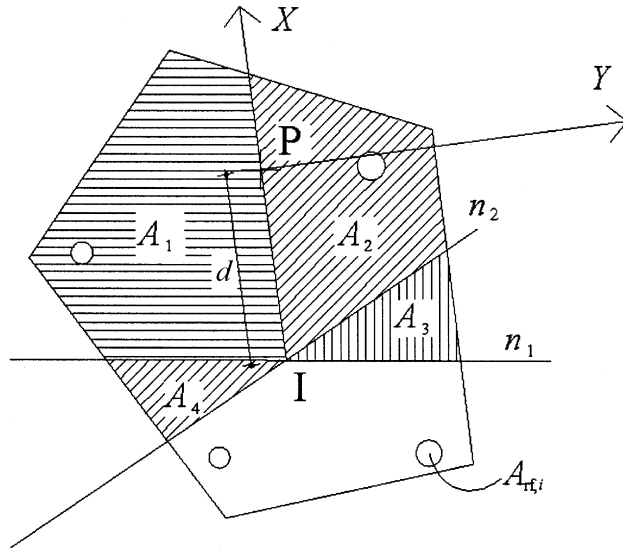## 2.2. Uniqueness of the fixed point

We prove the uniqueness of solutions by the proof of contradiction: we assume there are two different stress distributions fulfilling the conditions of equilibrium; the corresponding neutral axes are denoted by n_1 and n_2 (Fig. 3). In this proof we do not assume linear stress–strain relation, i.e., the value of k in Eq. (7) is arbitrary. The $[XY]$ global coordinate system is located so that the X-axis contains the intersection point I of lines n_1 and n_2 (having two parallel lines, the X-axis is parallel with them, respectively). We denote the regions of the cross section shown in Fig. 3 by $A_1, \ldots, A_4$. (If the point I is out of the convex boundary of the cross section, then A_3 or A_4 is an empty set.) The stresses at each point can be multiplied with a constant number; in this way the stress of the concrete at the point P can be 1 unit. The stress bodies belonging to the neutral axes are the following:

$$\sigma_1 = \begin{cases} \left(1 + \dfrac{1}{d} X + b_1 Y\right)^k & \text{if } (X, Y) \in A_1 \cup A_2 \cup A_3 \\[2ex] n\left(1 + \dfrac{1}{d} X + b_1 Y\right)^k & \text{if } (X, Y) \in A_{\mathrm{rf}} \\[2ex] 0 & \text{otherwise} \end{cases}, \qquad (10)$$

$$\sigma_2 = \begin{cases} \left(1+\dfrac{1}{d}X + b_2 Y\right)^k & \text{if } (X,Y) \in A_1 \cup A_2 \cup A_4 \\[2mm] n\left(1+\dfrac{1}{d}X + b_2 Y\right)^k & \text{if } (X,Y) \in A_{\mathrm{rf}} \\[2mm] 0 & \text{otherwise} \end{cases}, \qquad (11)$$

where d is the distance between points I and P. Without restricting generality, we can assume that $b_1 > b_2$, leading to $(\sigma_1 - \sigma_2) \geq 0$ for $Y \geq 0$. We introduce a new stress body:

$$\sigma^* = \begin{cases} \left(1+\dfrac{1}{d}X + b_1 Y\right)^k & \text{if } (X,Y) \in A_1 \\[2mm] \left(1+\dfrac{1}{d}X + b_2 Y\right)^k & \text{if } (X,Y) \in A_2 \\[2mm] n\left(1+\dfrac{1}{d}X + b_1 Y\right) & \text{if } (X,Y) \in A_{\mathrm{rf}} \\[2mm] 0 & \text{otherwise} \end{cases}. \qquad (12)$$

Fig. 3. The areas and notations distinguished in the text.

101

The bending moment of the stress body σ^* around the X-axis is denoted by M_0. The bending moments of σ_1 and σ_2 around the X-axis are denoted by M_1 and M_2. Since M_1 and M_2 must be zero, we obtain:

$$M_1 = \int_A \sigma_1 y \, dA = M_0 + \int_A (\sigma_1 - \sigma^*) y \, dA = M_0 + \int_{A_2 \cup A_3} (\sigma_1 - \sigma^*) y \, dA = 0, \quad (13)$$

$$M_2 = \int_A \sigma_2 y \, dA = M_0 + \int_A (\sigma_2 - \sigma^*) y \, dA =$$
$$M_0 + \int_{A_1 \cup A_4} (\sigma_2 - \sigma^*) y \, dA + \int_{A_{rf}} (\sigma_2 - \sigma^*) y \, dA = 0. \quad (14)$$

In the region $A_2 \cup A_3 (\sigma_1 - \sigma^*) \geq 0$ and $Y \geq 0$ the resulting M_0 must be negative. In the region $A_1 \cup A_4 (\sigma_2 - \sigma^*) \geq 0$ and $Y \leq 0$, for the reinforcement $(\sigma_2 - \sigma^*) \geq 0$ for $Y \leq 0$ and $(\sigma_2 - \sigma^*) \leq 0$ for $Y \geq 0$ the resulting M_0 must be a positive value. Consequently, Eqs (13) and (14) cannot be fulfilled for the same cross section. We reached a contradiction; the original assumption was false: there is only one neutral axis fulfilling the conditions of equilibrium. According to this proof, the 2D map has only one fixed point. In the next part we focus on the stability of this fixed point.

2.3. Local stability

The stability of the (X_0, Y_0) fixed point of the map given in Eq. (9) can be investigated by the $\lambda_1(X_0, Y_0)$ and $\lambda_2(X_0, Y_0)$ eigenvalues of the $\underline{\underline{L}}(X_0, Y_0)$ matrix of stability, where

$$\underline{\underline{L}}(X_0, Y_0) = \begin{pmatrix} \dfrac{\partial F}{\partial X} & \dfrac{\partial F}{\partial Y} \\ \dfrac{\partial G}{\partial X} & \dfrac{\partial G}{\partial Y} \end{pmatrix}\Bigg|_{X=X_0, Y=Y_0}. \quad (15)$$

If

$$\left| \lambda_1(X_0, Y_0) \right| \leq \left| \lambda_2(X_0, Y_0) \right| < 1, \quad (16)$$

then the fixed point is an attractor. We will show a coordinate system, where

$$\frac{\partial F}{\partial X}\bigg|_{\substack{X=X_0 \\ Y=Y_0}} = \frac{\partial G}{\partial X}\bigg|_{\substack{X=X_0 \\ Y=Y_0}} = \frac{\partial F}{\partial Y}\bigg|_{\substack{X=X_0 \\ Y=Y_0}} = \frac{\partial G}{\partial Y}\bigg|_{\substack{X=X_0 \\ Y=Y_0}} = 0. \quad (17)$$

Consequently,

$$\lambda_1 = \lambda_2 = 0, \quad (18)$$

as long as the map is differentiable. Since we compare the first and second moments of the area of arbitrary small regions, we neglect the reinforcement. We use the $[XY]$ global coordinate system, where $D_{xy} = 0$. The intersections of the neutral axis belonging to the fixed point with the convex boundary of the cross section are denoted by A and B (Fig. 4). Without restricting generality we can assume that $A \neq B$. For an asymmetric cross section and loading the line AB is typically not parallel with the axes of the $[XY]$ coordinate system. If they were parallel, the equations used in the proof would become more sophisticated, but the statement for the $\lambda_1(X_0, Y_0)$ and $\lambda_2(X_0, Y_0)$ eigenvalues would remain true. In this paper we give the proof for the typical case.

For the fixed point in the chosen global coordinate system the following is valid:

$$
\begin{bmatrix} X_0 \\ Y_0 \end{bmatrix} = \begin{bmatrix} \dfrac{I_{Y,0}}{S_{Y,0}} \\ \dfrac{I_{X,0}}{S_{X,0}} \end{bmatrix}.
\tag{19}
$$

The neutral axis can be given with

$$
Y = Y_0 - \frac{Y_0}{X_0} X.
\tag{20}
$$
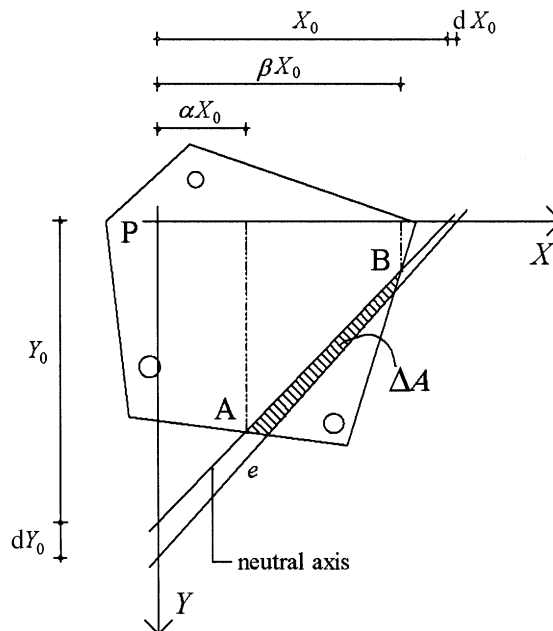
Fig. 4. Notations for the proof of stability.

103

A line, denoted by $e,$ is arbitrary close to the neutral axis:

$$Y = Y_0 + dY_0 - \frac{Y_0 + dY_0}{X_0 + dX_0} X. \tag{21}$$

The region of the cross section between the neutral axis and line e is denoted by $\Delta A.$ We introduce the following sign:

$$\int_{\Delta A} (.) dA \overset{def}{=} \int_{X=\alpha X_0}^{X=\beta X_0} \int_{Y=Y_0 - \frac{Y_0}{X_0} X}^{Y=Y_0 + dY_0 - \frac{Y_0 + dY_0}{X_0 + dX_0} X} (.) dy dx. \tag{22}$$

(The area calculated according to Eq. (22) differs from the area shaded in Fig. 4 only in the second terms.) By applying Eq. (22) the first and second moments of the area belonging to the line e can be given as follows:

$$S_X = \frac{I_{X,0}}{Y_0} + \int_{\Delta A} Y dA, \tag{23}$$

$$S_Y = \frac{I_{Y,0}}{X_0} + \int_{\Delta A} X dA, \tag{24}$$

$$I_X = I_{X,0} + \int_{\Delta A} Y^2 dA, \tag{25}$$

$$I_Y = I_{Y,0} + \int_{\Delta A} X^2 dA, \tag{26}$$

$$D_{XY} = \int_{\Delta A} XY dA. \tag{27}$$

Substituting these values into Eq. (9) and differentiating it by the computer program MAPLE, we gain the following results on the partial derivatives:

$$\left. \frac{\partial F}{\partial dX_0} \right|_{\substack{dX_0=0 \\ dY_0=0}} = \left. \frac{\partial F}{\partial dY_0} \right|_{\substack{dX_0=0 \\ dY_0=0}} = \left. \frac{\partial G}{\partial dX_0} \right|_{\substack{dX_0=0 \\ dY_0=0}} = \left. \frac{\partial G}{\partial dY_0} \right|_{\substack{dX_0=0 \\ dY_0=0}} = 0. \tag{28}$$

The partial derivatives are independent of α and $\beta.$ This enables us to extend the proof for concave cross sections, where the line AB contains points not belonging to the cross section. In this case ΔA contains more, detached areas, bordered by $\alpha_1 \cdot X_0$ and $\beta_1 \cdot X_0,$ $\alpha_2 \cdot X_0$ and $\beta_2 \cdot X_0,$ ..., etc. Equations (23)–(27) must be modified according to these conditions. After the substitutions and partial derivations we gain the results of Eq. (28). We find that all of the elements

and the eigenvalues of the matrix of stability are zero, the fixed point is (super)stable.

2.4. Partial results on global stability

In numerical simulations we found that the map given in Eq. (9) was globally convergent. We give a proof for global convergence for symmetric cross sections under compression and uniaxial bending. This case can be associated with a 1D map provided the first estimation on the neutral axis is perpendicular to the axis of symmetry. Although we were unable to extend this proof for the general two-dimensional case, we are convinced that a similar mechanism governs the iteration.

A load is applied to the axis of symmetry of the cross section at the point P. We assume that the point P is outside the kernel of the cross section, but is inside its convex boundary. (If it is inside the kernel, we have a neutral axis out of the cross section; for this case we have to solve the equilibrium equations only once.) The X-axis of the global coordinate system is at the axis of symmetry; its direction is given in such a way that the X coordinate of the C centroid is positive. Due to the symmetry the estimations on the neutral axis and the final solution are parallel to each other. The iteration can be given as

$$X^i = f(X^{i-1}) = \frac{I_y^{i-1}}{S_y^{i-1}}. \tag{29}$$

We will investigate the convergence properties of the map given in Eq. (29). At each step of the iteration the cross section is cut into a maximum of two parts by the current estimation on the neutral axis. We solve Eq. (29) for the working cross section part, i.e., the part containing the point P. Due to our assumptions there must be an estimation, where the S_y statical moment of the working cross section part is zero. This estimation is denoted by e_2. If the estimation for the neutral axis is between the Y-axis and e_2, S_y is negative, otherwise it is positive. I_y is a positive number for any estimation. It means that $f(X)$ has a singularity at $X = e_2$. Due to the rule that the working cross section part always contains the point P, there is another singularity at $X = 0$. Except the two singularities, $f(X)$ is continuous. Summing up, we have the following statements for the sign of $f(X)$:

$$f(X) > 0 \qquad \text{if} \qquad X < 0 \text{ or } X > e_2, \tag{30}$$

$$f(X) < 0 \qquad \text{if} \qquad 0 < X < e_2, \tag{31}$$

$$\lim_{X \to e_{2^-}} f(X) = -\infty, \tag{32}$$

$$\lim_{X \to e_{2^+}} f(X) = +\infty. \tag{33}$$

To determine the shape of $f(X)$, we investigate the first derivative by assuming there is a limit point, where

$$f(X + \mathrm{d}X) = f(X). \tag{34}$$

The last equation can be written as

$$\frac{I_y + \mathrm{d}X \cdot h \cdot (X + \mathrm{d}X/2)^2}{S_y + \mathrm{d}X \cdot h \cdot (X + \mathrm{d}X/2)} = \frac{I_y}{S_y}, \tag{35}$$

where h is the height of the arbitrary narrow slice according to Fig. 5. Neglecting the higher terms in $\mathrm{d}X$ and solving Eq. (35), we obtain that the first derivative can be zero if and only if

$$X = \frac{I_y}{S_y}. \tag{36}$$

By the proof of the uniqueness of solutions there must be one point where $X = f(X)$; this point is denoted by X_0. Equations (30) and (31) ensure that $X_0 > e_2$, by Eq. (36) at this point $f'(X) = 0$. Making an inequality from Eqs (35) and (36), we can state

1) for $S_y > 0$

        if $f(X) < X$,   then $f(X)$ increases monotonously,

        if $f(X) > X$,   then $f(X)$ decreases monotonously;

2) for $S_y < 0$

        if $f(X) < X$,   then $f(X)$ decreases monotonously,

        if $f(X) > X$,   then $f(X)$ increases monotonously.
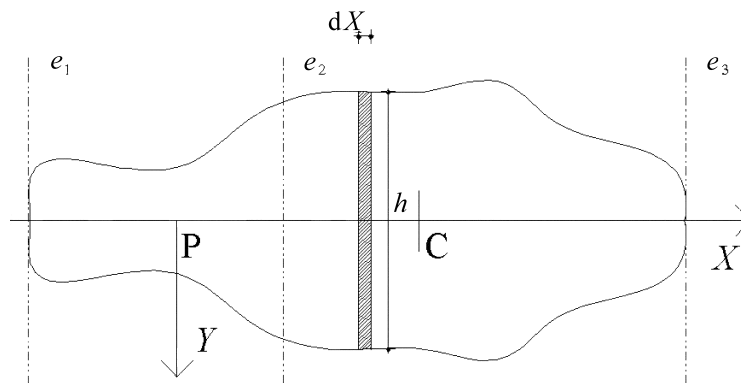

Fig. 5. A symmetric cross section.

These statements ensure that there cannot be more limit points than X_0. To show the shape of $f(X)$, we take the e_1 and e_3 borders of the cross section into account. The function $f(X)$ can be written as follows:

$$X \in [-\infty, e_1] \qquad f(X) = c_0, \tag{37}$$

$$X \in (e_1, 0] \qquad 0 < f(X + dX) < f(X), \tag{38}$$

$$X \in (0, e_2] \qquad f(X + dX) < f(X) < 0, \tag{39}$$

$$X \in (e_2, X_0] \qquad 0 < f(X + dX) < f(X), \tag{40}$$

$$X \in (X_0, e_3] \qquad 0 < f(X + dX) < f(X), \tag{41}$$

$$X \in (e_3, +\infty] \qquad f(X) = c_0, \tag{42}$$

where c_0 is a positive constant. The shape of $f(X)$ is given in Fig. 6. The only fixed point is at X_0. Since $f(X)$ rises monotonously in $(X_0, e_3]$ and is constant for $X > e_3$, the iteration started at $X > X_0$ definitely converges to a fixed point and cannot produce $X < X_0$. One can show that the iteration started elsewhere gets into this convergent region in a finite number of iterative steps, but detailed proof is omitted in this paper.
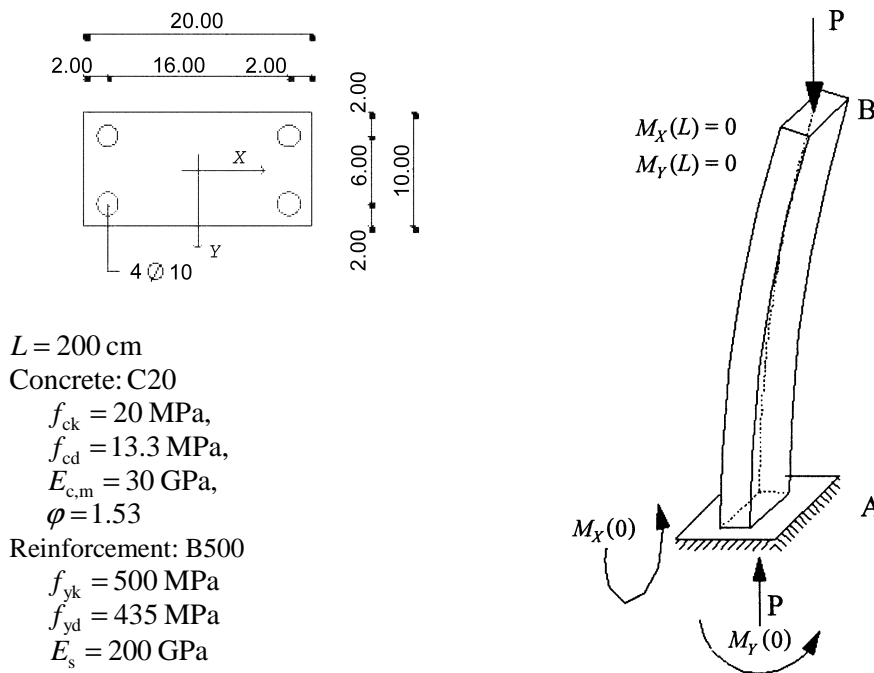
For the general, two-dimensional map we carried out systematic search for a counterexample, but were unable to find any. The map was globally convergent even for very extreme cases.
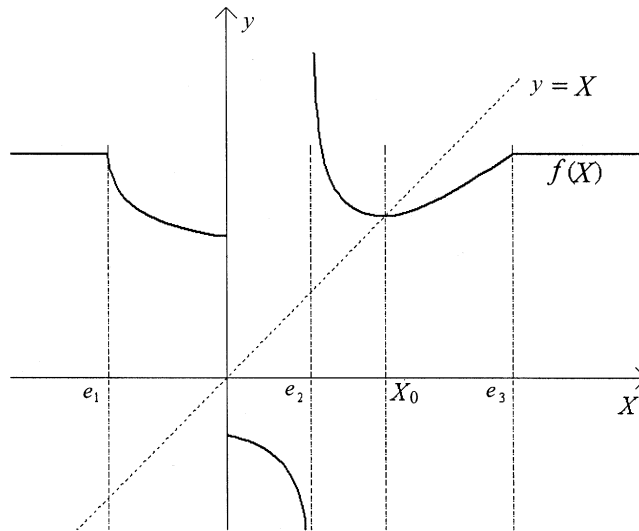
Fig. 6. The *f(X)* function.

3. CALCULATION OF SPATIAL DEFORMATIONS USING THE ITERATIVE SCHEME

In our calculations we use the third-order theory, i.e., full geometric non-linearity. The described iterative scheme is used to locate the neutral axis in each cross section. Subsequently the curvature is integrated along the beam axis from $s = 0$ to $s = L$. This integrator can be viewed as a set of algebraic *functions* f_i. The variables v_j are the nonconstant boundary conditions at $s = 0$, the function values are the prescribed conditions at $s = L$. As a simple example, let us consider a homogeneous, linearly elastic cantilever, loaded by the compressive force F (Fig. 7). In this example we have three variables, F and the initial bending moments $M_X(0)$ and $M_Y(0)$. The far-end values $M_X(L)$ and $M_Y(L)$ can be viewed as *functions* $f_1(F, \ M_X(0), \ M_Y(0))$ and $f_2(F, \ M_X(0), \ M_Y(0))$ assuming that an integrator is available. Now we seek the solutions of $f_1 = f_2 = 0$. In general, we have n functions and $n + 1$ variables; the latter define the *Global Representation Space* (GRS) of the problem. A fast and efficient parallel algorithm, the PHA is presented in [11] for solving such a system of equations.


$L = 200\,\mathrm{cm}$
Concrete: C20
$\quad f_{ck} = 20\,\mathrm{MPa},$
$\quad f_{cd} = 13.3\,\mathrm{MPa},$
$\quad E_{c,m} = 30\,\mathrm{GPa},$
$\quad \varphi = 1.53$
Reinforcement: B500
$\quad f_{yk} = 500\,\mathrm{MPa}$
$\quad f_{yd} = 435\,\mathrm{MPa}$
$\quad E_s = 200\,\mathrm{GPa}$

Fig. 7. An axially loaded cantilever beam with its cross section. Abbreviations: f_{cd}, design value of the compression strength of the concrete; f_{ck}, characteristic value of the compression strength of the concrete; f_{yk}, characteristic value of the yield stress of the reinforcement; f_{yd}, design value of the yield stress of the reinforcement; φ, the creep coefficient; $E_{c,m}$, the mean value of the elastic modulus for the concrete; E_s, the elastic modulus for the reinforcement.

The PHA computation starts with the discretization of the GRS by choosing a simplicial grid. In a two-dimensional case this simplicial grid contains triangles. The function f_i is evaluated at the meshpoints and linearly interpolated in the simplectic domains. Since the calculation of two simplexes is independent, the computation can be carried out in a parallel environment.

The simplex algorithm was implemented under the Parallel Virtual Machine (PVM). A great advantage of the simplex method is that only the finite-dimensional GRS points of the bifurcation diagram are stored, not the final shape of the bar. The latter can be easily computed by integration for a selected point of the bifurcation diagram. Figure 8 shows the bifurcation diagram belonging to the cantilever beam.

In this article we emphasize the theoretical background of the proposed method. The material properties of steel reinforced concrete can be taken into account according to the EC2 standard. These modifications do not influence the convergence properties of the recursion and the robustness of the PHA. By these extensions the method is capable of calculating deformations of columns under compression and biaxial bending or the deflections of prestressed beams in the Serviceability Limit States. It can be used for designing cross sections of columns joint together in a frame structure in the Ultimate Limit States taking the effective stiffness of the bar into account.
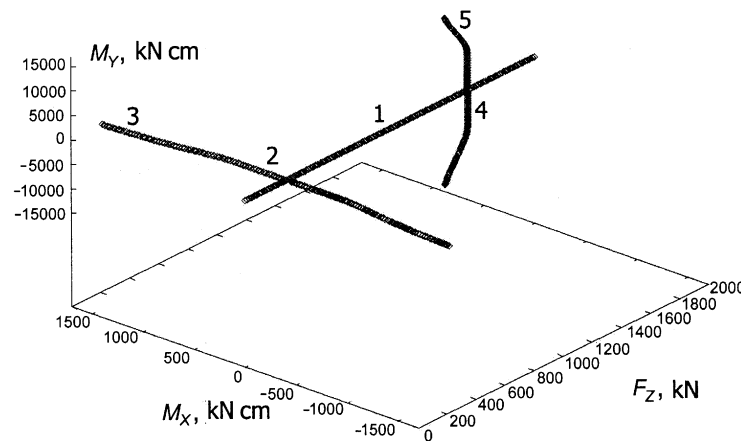
Fig. 8. The bifurcation diagram belonging to the cantilever beam in Fig. 7. 1, the trivial solution; 2, the first buckling mode in the weaker direction (a stable bifurcation not influenced by the limited tensile strength); 3, the decreasing part of the same branch due to the cracking; 4, the first buckling mode in the stronger direction; 5, the decreasing part of the same branch.

4. SUMMARY

In this paper a method is presented for calculating spatial deformations of reinforced concrete bars. The core of the algorithm is a globally convergent recursion, which determines the neutral axis of an arbitrary reinforced concrete cross section. The proof for the uniqueness of solutions, the stability of the only fixed point, and the global convergence for symmetric cross sections are given. The recursion can be used in the PHA, which is an efficient solver of boundary value problems. A cantilever beam under axial compression is presented as an example.

ACKNOWLEDGEMENTS

REFERENCES

1. Domokos, G. Global description of elastic bars. *Z. Angew. Math. Mech.*, 1994, **74**, T289–T291.
2. Domokos, G. A group-theoretic approach to the geometry of elastic rings. *J. Nonlin. Sci.*, 1995, **5**, 453–478.
3. Domokos, G. and Gáspár, Zs. A global, direct algorithm for path-following and active static control of elastic bar structures. *Int. J. Struct. Mech.*, 1995, **23**, 549–571.
4. Gáspár, Zs. The form of an ideally elastic bar with a space curve axis. *Acta Techn. Hung. Acad. Sci.*, 1977, **84**, 293–306.
5. Li, Y. and Maddocks, J. On the computation of equilibria of elastic rods, part I: Integrals, symmetry and a Hamiltonian formulation. *J. Comput. Phys.* (submitted).
6. Coleman, B. D., Tobias, I. and Swigon, D. Theory of the influence of the end-conditions on the self-contact in DNA loops. *J. Chem. Phys.*, 1995, **103**, 9101–9109.
7. Swigon, D., Coleman, B. D. and Tobias, I. The elastic rod model for DNA and its application to tertiary structure of DNA minicircles in mononucleosomes. *Biophys. J.*, 1998, **74**, 2515–2530.
8. McMillien, T. and Goriely, A. Tendril perversion in intrinsically curved rods. *J. Nonlin. Sci.*, 2002, **12**, 241–281.
9. Goriely, A. and Tabor, M. The mechanics and dynamics of tendril perversion in climbing plants. *Phys. Lett.*, 1998, **A250**, 311–318.
10. Brøndum-Nielsen, T. Serviceability limit state analysis of cracked, polygonal concrete sections under biaxial or symmetric bending. *ACI Journal*, 1986, **83**, 209–218.
11. Domokos, G. and Szeberényi, I. A hybrid parallel approach to one-parameter nonlinear boundary value problems. *Comput. Assist. Mech. Eng. Sci.*, 2004, **11**, 15–34.
12. Gáspár, Zs., Domokos, G. and Szeberényi, I. A parallel algorithm for the global computation of elastic bar structures. *Comput. Assist. Mech. Eng. Sci.*, 1997, **4**, 55–68.

Tõmbetugevuseta materjalist varraste ruumiliste deformatsioonide arvutamise robustne algoritm

András A. Sipos

On esitatud globaalselt koonduv iteratiivne algoritm elastsete tõmbetugevu-seta materjalist talade ruumiliste deformatsioonide arvutamiseks. Algoritmi tuumaks on iteratiivne skeem neutraaltelje asukoha ja seega ka varda kõveruse määramiseks (lähtudes Kirchhoffi klassikalisest vardateooriast). Üldjuhu jaoks on tõestatud tulemuse ühesus ja lokaalne stabiilsus, sümmeetriliste ristlõigete jaoks on tõestatud globaalne stabiilsus. Skeem on sisestatud iteratsioonivabasse globaalse ääreväärtuse ülesande lahendajasse (nn paralleelne hübriidalgoritm), määramaks ruumilist tasakaalukuju. Ilmseks rakenduseks on eelpingestatud või eelpingestamata raudbetoontalade ja -postide arvutamine.